行政院國家科學委員會專題研究計畫成果報告

複雜薄膜表面與隱藏式介面的非線性分子振動光譜研究 (II)

計畫類別：☑個別型計畫　□整合型計畫

計畫編號：NSC 88 —2112—M009—036

執行期間：88 年 8 月 1 日至 89 年 7 月 31 日

個別型計畫：計畫主持人：黃中垚
共同主持人：

整合型計畫：總計畫主持人：
子計畫主持人：

註：整合型計畫總報告與子計畫成果報告請分開編印各成一冊，彙整一起繳送國科會。

處理方式：☑可立即對外提供參考
（請打ｖ）□一年後可對外提供參考
□兩年後可對外提供參考
（必要時，本會得展延發表時限）

執行單位：國立交通大學光電工程研究所

中華民國 89 年 10 月 31 日

複雜薄膜表面與隱藏式介面的非線性分子振動光譜研究 (II)

計劃編號: NSC89-2112-M-009-036

執行期限: 民國八十八年八月一日至八十九年七月三十一日

主持人: 黃中垚

傳真: 03-5716631

電子郵遞地址: jyhuang@cc.nctu.edu.tw

執行機關: 交通大學光電工程研究所

摘要

在本年度報告中我們報導分子振動光譜技術的發展與在複雜薄膜方面的應用。在第二年研究期間我們完成和頻振動光譜、時析偏極化紅外吸收光譜、拉曼散射與成像等技術並將之應用於液晶和高分子配向膜。有關此材料體系應用的重要問題是液晶分子如何排列和其受電場誘導轉向的詳細過程。我們從液晶分子有序排列和轉向過程的光譜資訊，以試圖建構完整的分子尺度模型。未來希望能利用所建立的光譜分析方法探討分子手徵性如何影響鐵電性與反鐵電性液晶薄膜的電場誘導轉向的詳細過程。

Nonlinear Molecular Vibrational Spectroscopy for Surface Analysis of Thin Complex Films and Buried Interfacial Systems (II)

NSC89-2112-M-009-036 (Aug. 1, 1999 to July 31, 2000)

Investigator: Jung Y. Huang
Organization: Institute of Electro-Optical Engineering
Chiao Tung University
Hsinchu, Taiwan 30050, R.O.C.
Tel: 03-5719755
Fax: 03-5716631
E-mail: jyhuang@cc.nctu.edu.tw

Abstract

In this report, we present the studies of thin complex films, such as liquid crystals and polymeric aligning layers, with optical retardance measurement, infrared absorption spectroscopy, Raman scattering, and Raman imaging microscopy. The molecular ordering of liquid crystals and polymeric thin films induced by mechanical rubbing and ultraviolet light exposure are investigated in view of their technical potential. An important question is that how liquid crystal molecules are aligned and reoriented during field-induced switching. It is still unclear about the detailed reorientation process of the chain and core parts of liquid crystal. To understand the underlying dynamics at the molecular level, we are employing Fourier transform infrared absorption spectroscopy to generate time-resolved spectra of liquid crystal molecules during the field-induced switching process. By combining these methods we wish in the near future to answer how molecular chirality and chiral dopants affect the switching dynamics of ferroelectric liquid crystals.

Contents

I. Introduction

Functional thin complex films such as polymers, liquid crystals, and ferroelectric materials, possess high application potential. However, usefulness of these thin film systems critically depends upon the spatial distributions of the constituents and their orientation alignment. The information unfortunately is quite difficult to be obtained. We are conducting a multi-years research program for developing a variety of techniques of spectroscopy and microscopy to attack this difficulty. These tools are specifically designed for probing the inhomogeneous distribution of functional thin complex films.

During the second-year effort, several tools had been designed, constructed, and tested their capabilities in serving our purpose. These techniques include optical retardance measurement, polarized and time-resolved Fourier-transform infrared (FTIR) absorption spectroscopy, infrared-visible sum-frequency (IVSFG) vibrational spectroscopy, and Raman spectroscopy and imaging microscopy.

With the optical retardance measurement set up, anisotropy in the plane of thin films can be deduced. The in-plane optical anisotropy usually reflects the distribution of molecular segments that possess polarizable electronic structure and contribute significantly to the index of refraction. To answer which functional groups are involved in the optical anisotropic distribution; polarized FTIR with its molecular specificity is employed to provide more detailed picture. Usually structure and orientation of atomic groups on thin complex films determined their application properties. An analytical tool with surface sensitivity and molecular specificity is highly demanded. These requirements can be met with infrared-visible sum-frequency vibrational spectroscopy. Direct imaging of the infrared absorption and Raman scattering signals can yield the two-dimensional distribution of specific atomic groups in thin complex films, is therefore highly useful for probing thin complex films. We demonstrate these spectroscopic imaging techniques at the micrometer scale to be feasible.

Finally, to investigate the molecular dynamics of a field-induced reorientation in a thin complex liquid crystal film, we are currently undergoing to construct a time-resolved FTIR spectroscopy to probe the underlying reorientation process at the molecular level. In the near future, we hope by combining these methods to answer how molecular chirality and chiral dopants affect the switching dynamics of ferroelectric liquid crystals.

Theory

(a) Polarized infrared absorption and the relations to the order parameters of molecular orientational distribution

A laser beam propagates through a sample, which has a complex index of refraction $\tilde{n}(\neg) = n(\neg) - iK(\neg)$, will experience an intensity loss of

$$-dI = K(\neg) I\, dl = \frac{h\neg}{c} B_{n'n''}(N_{n''} - N_{n'}) I\, dl \ , \qquad \text{(IIa.1)}$$

where $N_{n'}$ is the population of the n' level. B is the Einstein B coefficient of the material and can be related to the square of the transition moment from n' to n''

$$B_{n'n''} = \frac{(2®)^3}{3h^2}[\,|(«_x)_{n'n''}|^2 + |(«_y)_{n'n''}|^2 + |(«_z)_{n'n''}|^2] = \frac{(2®)^3}{3h^2}|(«)_{n'n''}|^2 \ . \qquad \text{(IIa.2)}$$

From Eqs. (IIa.1) and (IIa.2), the extinction coefficient K(ν) can be then expressed as

$$K(\neg) = \frac{(2®)^3}{3ch}\neg_{n'n''}(N_{n''} - N_{n'})\,|(«)_{n'n''}|^2 \ . \qquad \text{(IIa.3)}$$

Assuming $B_{n'n''}$ to be constant over the spectral line, we then have an integrated absorption coefficient of

$$\int K(\neg)d\neg = \frac{N®}{3c} <|(«_g)_{n'n''}|^2> \ , \qquad \text{(IIa.4)}$$

where $«_g = «_g^{(0)} + \sum_K «_g^{(K)} Q_K$.

A 2nd-rank absorbance tensor can be defined as

$$A(\Phi) = \frac{N®}{3c}\int [«_g^{(K)} \cdot \hat{E}]^2 f(\Omega) d\Omega \quad , \qquad \text{(IIa.5)}$$

where Φ is the angle between the incident light polarization direction and the X-axis of the laboratory coordinates system, $f(\Omega)$ denotes the orientational distribution of the dipole moment derivative in the measurement spot. We can also deduce an anisotropic part from the absorbance tensor

$$a_{ik} = A_{ik} - \frac{1}{3} Tr(A_{ik}) \delta_{ik} \quad . \qquad \text{(IIa.6)}$$

In the molecular frame, the anisotropic absorbance tensor can be expressed in terms of an 1×5 vector

$$W^{mol} = (\sqrt{3/2}\, a_{ss}, \sqrt{1/2}\,(a_{\zeta\zeta} - a_{\eta\eta}), \sqrt{2}\, a_{\zeta\eta}, \sqrt{2}\, a_{\zeta\xi}, \sqrt{2}\, a_{\eta\xi}) \ . \qquad \text{(IIa.7)}$$

Similarly, in the laboratory frame, the corresponding anisotropic absorbance tensor can be found to be: $W^{lab} = (\sqrt{3/2}\, a_{zz}, \sqrt{1/2}\,(a_{xx} - a_{yy}), \sqrt{2}\, a_{xy}, \sqrt{2}\, a_{xz}, \sqrt{2}\, a_{yz})$. (IIa.8)

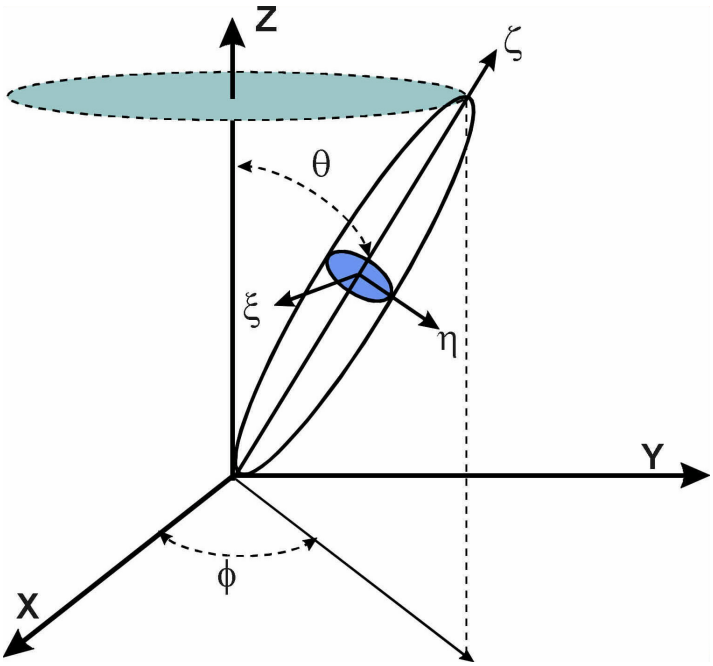

Fig. IIa.1 Schematic *diagram showing the relationship between the molecular frame (ζ,η,ξ) and the laboratory coordinates system (XYZ).*

From Eq. (IIa.5) we can obtain simple relationships between the orientational averaged absorbance tensors from the molecular to the laboratory frames

$$< W_l^{lab} >= \int W_l^{lab} f(\Omega) d\Omega = \int W_l^{mol} S_{ml} f(\Omega) d\Omega = < W_m^{mol} >< S_{ml} > . \qquad \text{(IIa.9)}$$
$$where\ m,\ l = 1, 2, ..., 5$$

With a normal incident geometry on the XZ plane, the integrated absorbance is found to be

$$A(\Phi) = \frac{1}{3} A - \frac{1}{2}\sqrt{\frac{2}{3}}\, W_1^{lab} + \sqrt{2}\, W_2^{lab} < \cos 2\Phi > \quad . \qquad \text{(IIa.10)}$$

Based on the analysis, the orientational distribution of given functional groups in a complicated thin film can be deduced from a set of measured polarized Fourier-transform infrared (FTIR) absorption spectra. The procedure is detailed as follows:

(i) *For a given normal mode vibration the integrated absorbance as a function of the incident infrared polarization direction A(c) is first calculated from measured FTIR spectra*;

(ii) *Fit the resulted A(c) to Eq. (IIa.10) to deduce* W_1^{lab} *and* W_2^{lab};

(iii) *From*

$$\begin{aligned} W_1^{lab} &= \sqrt{3/2}\ a_Z = W_1^{mol} < S_{11} > + W_2^{mol} < S_{21} > \\ W_2^{lab} &= \sqrt{1/2}\ (a_X - a_Y) = W_1^{mol} < S_{12} > + W_2^{mol} < S_{22} > \end{aligned} \qquad \text{(IIa.11)}$$

and

$$\begin{aligned} W_1^{mol} &= \sqrt{3/2}\ (\alpha_{g,s}^{(K)})^2 \\ W_2^{mol} &= \sqrt{1/2}\ [(\alpha_{g,\parallel}^{(K)})^2 - (\alpha_{g,\perp}^{(K)})^2] \end{aligned}$$

(IIa.12)

the order parameters of molecular distribution, $< S_{11} >, < S_{12} >, < S_{21} >$, *and* $< S_{22} >$, *can then be determined*. Note that $< S_{11} >$ *and* $< S_{12} >$ denote the orientational order parameter and the transverse order parameter (which relates to the dichroic ratio), and $< S_{21} >$ *and* $< S_{22} >$ can reflect the biaxiality of the film.

(b) Raman scattering and the relations to the order parameters of molecular orientational distribution

Considering a molecule which is excited by a laser beam with a polarization along the X-axis and propagating along the Y-axis of the laboratory frame, the Raman signal along the Z-axis is proportional to

$$I_s(\theta_s, \theta_p) = \frac{2\pi^3 \theta_p \theta_s^3}{\lambda}[< \alpha_Y^2(Q) > + < \alpha_Z^2(Q) >] = \frac{2\pi^3 \theta_p \theta_s^3}{\lambda}[< \gamma_{YX}^2 > + < \gamma_{XX}^2 >]. \quad \text{(IIb.1)}$$

The Raman polarizability tensor for a rod-shape molecule usually possesses a single dominant component γ_{ss}. A free molecular rotation along the s-axis leads to the following orientational averages of the squared polarizability components

$$< \sim_{YX}^2 >= \sin^4 \Phi [\cos\Phi\cos\alpha - \sin\Phi\sin\alpha]^4 \sim_{ss}^2$$

$$< \sim_{YX}^2 >= \frac{1}{4}\sin^4 \Phi [2\cos\Phi\sin\Phi\cos(2\alpha) + (\cos^2\Phi - \sin^2\Phi)\sin(2\alpha)]^2 \sim_{ss}^2$$

(IIb.2)

Here Φ is the azimuthal angle between the sample coordinates (xyz) and the laboratory frame (XYZ). By combining Eqs. (IIb.1) and (IIb.2), we therefore obtain the azimuthal-dependent Raman scattering intensity

$$I_s(\neg_s, \neg_p) = I_{s0}[1 + < \cos(2\alpha > \cos(2\Phi)] = I_{s0}[1 + Q \cdot \cos(2\Phi)], \qquad \text{(IIb.3)}$$

where Q is the azimuthal order parameter. Eq. (IIb.3) will be used to deduce the aligning ordering of liquid crystal molecules on a variety of polymeric surfaces.

II. Experimental developments for characterizing thin complex films

(a) Characterization of polymeric aligning surfaces with optical retardation measurement

The molecular orientation of polymers can be studied using wide-angle x-ray diffraction, small-angle x-ray diffraction, polarized infrared absorption spectroscopy, and birefringence measurements. Birefringence measurements are quite robust because they can determine molecular orientation for both amorphous and crystalline materials. The angle between the polymer chains and the film in-plane direction govern the anisotropy. The birefringence Δn of spin-coated films can be related to their molecular orientation $Q =< \cos(2\alpha) >$ using

$$\Delta n = n_{\parallel} - n_{\perp} = \frac{\Delta n_{\max}}{4}(3Q + 1) \qquad \text{(IIIa.1)}$$

where $n_{\parallel}$ is the index of refraction lateral to the film, $n_{\perp}$ is the index of refraction vertical to the film, and $\Delta n_{\max}$ is the maximum birefringence at perfect molecular alignment which yields Q=1.

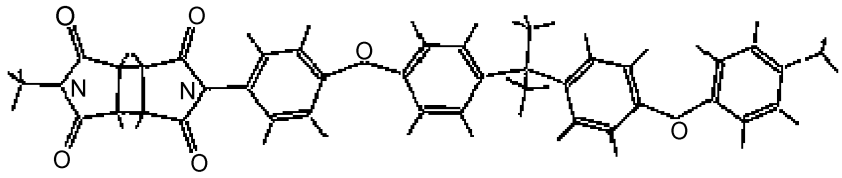

Fig. IIIa.1 *Chemical structure (top) of a polyimide (RN-1182, Nissan Chemicals) used in this study*

We prepared a polyimide film with an in-plane anisotropy. The film was subjected to uniaxial rubbing with a rotating velvet wrapped roller. The resulting in-plane anisotropy was investigated with an optical retardance measurement. The result is present in Fig. IIIa.2 with the filled circles. Apparently, the imide and benzene rings, which are believed to be the species that contribute significantly to the index of refraction of the film. The order parameter is fairly high with a magnitude of Q=0.72, indicating these rings are aligned very well by the mechanical rubbing process.

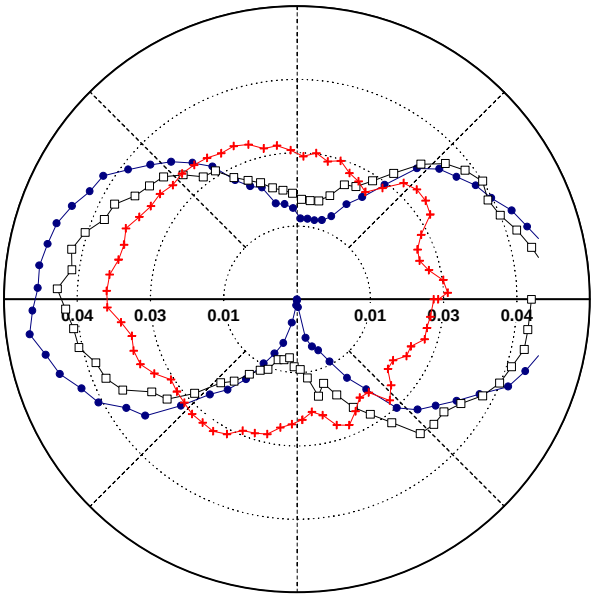

Fig. IIIa.2 *In-plane index of refraction change in the polyimide film measured with optical retardance method. Filled circles (blue): rubbed film, open squares: the same film was exposed to unpolarized ultraviolet light (a¼ 250 ì 310 nm) with 147 mJ/cm², and red crosses: with exposure 2940 mJ/cm².*

The uniaxial alignment can be removed completely by exposing the rubbed film to unpolarized ultraviolet light (λ~250$\rightarrow$310 nm) with an exposure of 2940 mJ/cm^2 (see the curve of the red crosses in Fig. IIIa.2). Therefore the film has the potential as an aligning layer of liquid crystal device especially when photoalignment technique is employed. To reveal the detailed process of the polyimide molecule with ultraviolet light, infrared absorption and Raman scattering measurements on the alignment layers and liquid crystal cells were employed and the results are presented as follows.

(b) Characterization of polymeric aligning films with Fourier transform infrared absorption spectroscopy

Fourier-transform infrared absorption spectra of RN-1182 polyimide and the film exposed to UV light with exposures of *0 (blue), 147 mJ/cm^2 (red), and 1029 mJ/cm^2 (green) are* presented in Fig. IIIb.1. Three major peaks at 1721 cm^{-1}, 1501 cm^{-1} and 1238 cm^{-1} can be attributed to the C=O stretch of the imide ring, C-O-C and C=C stretches of the ϕ-O-ϕ structure, respectively. Two other vibration features with one at 1381 cm^{-1} and the other at 1154 cm^{-1} are modified by UV exposure. Based on our *ab initio* calculation using density functional theory, we are able to assign these two peaks to the symmetric and antisymmetric stretches of C-N-C of the imide ring. The peak at 1381 cm^{-1} was found to upshift to 1397cm^{-1} and the other peak at 1173 cm^{-1} downshift to 1154 cm^{-1} after UV light exposure.

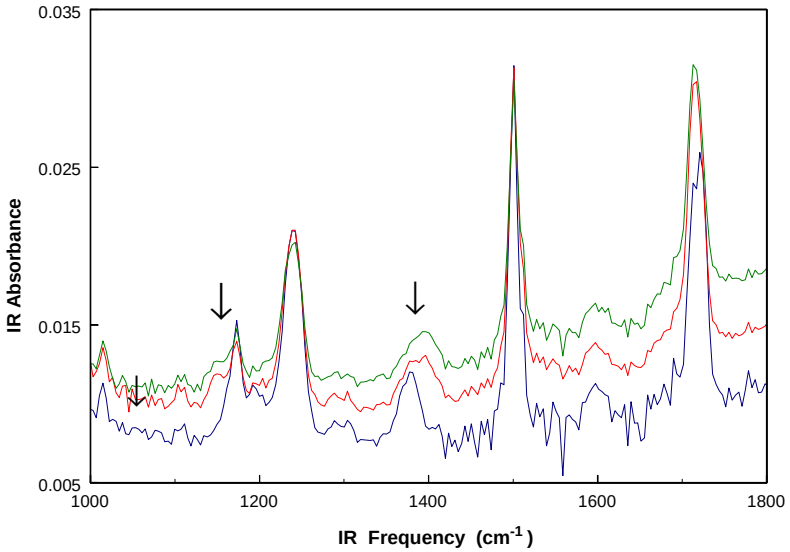

Fig. IIIb.1 *Fourier transform infrared absorption spectra of the polyimide film which had been subjected to varying exposures (blue: 0, red: 147 mJ/cm² , and green: 1029 mJ/cm²) of ultraviolet light with ª¼ 250 ì 310 nm.*

It has been known that imide ring is photoactive and can be modified by UV absorption. A simple model can therefore be proposed, which is illustrated by a schematic diagram of Fig. IIIb.2. The separation of the connected imide rings leads to a rearrangement of the RN-1182 polymer chain and therefore removes the rubbing-induced in-plain anisotropy. A similar exposure on a spin-coated RN-1182 film with polarized UV light can also produce an in-plane anisotropy.

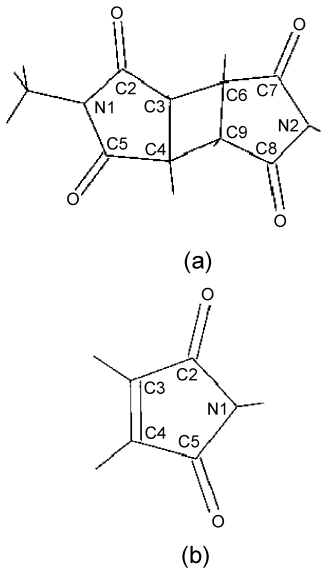

Fig. IIIb.2 *A chemical reaction model proposed to explain the observed infrared absorption spectra shown in Fig. IIIb.1*

To probe more deeply what happen on the rubbed RN-1182 film, we employed infrared-visible sum-frequency (IVSFG) vibrational spectroscopy to reveal the realigned surface structure. The result is presented in Fig. IIIb.3, where shows the CH_3 stretch of the RN-1182 segments on surface. The peak at 2881 cm^{-1} is originated from the symmetric stretch of CH3 on Phe-O-Phe segment of RN-1182 molecule. The azimuthal dependence of the peak intensity along the surface normal clearly exhibits threefold symmetry along the rubbing direction. Since IVSFG process is high surface specific, the threefold symmetry of the azimuthal pattern indicates CH_3 group on the film surface is not isotropic. We currently are undertaking similar investigation on UV light exposed RN-1182 films with IVSFG spectroscopy in order to reveal the detailed surface aligning mechanism by UV photon absorption. The information is important for understanding the detailed photo alignment processes of liquid crystal by UV defined polyimide film. The results shall be presented in our next NSC annual report.

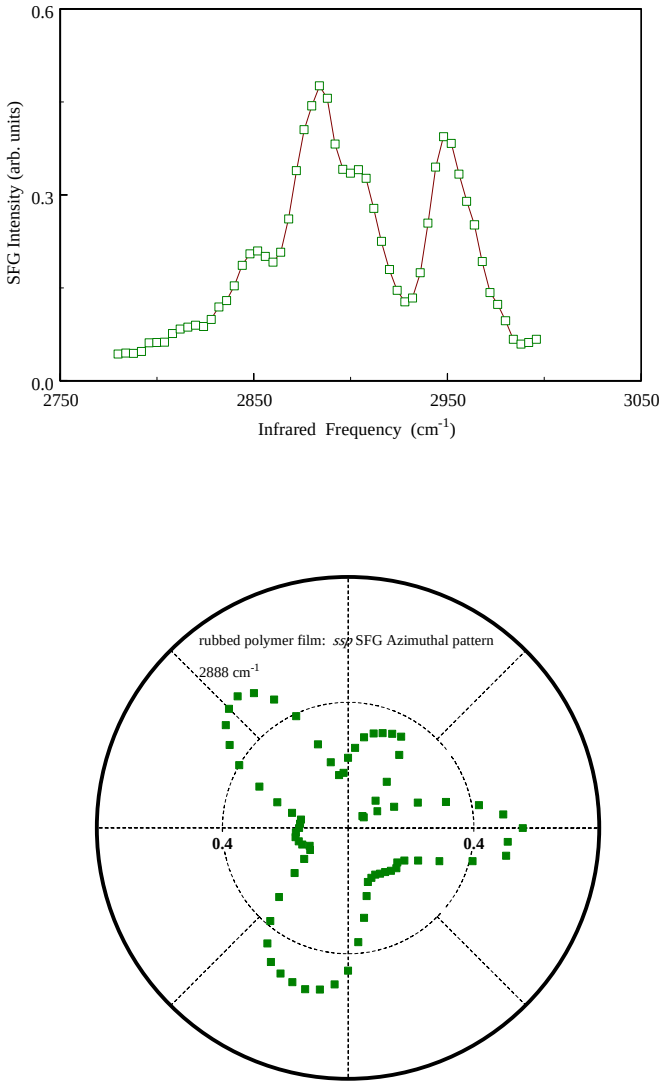

Fig. IIIb.3 *(Top) An infrared-visible sum-frequency vibrational spectrum from hydrocarbon segments of a RN-1182 film. (Bottom) Azimuthal dependence of the symmetric CH_3 stretch peak at 2881 cm^{-1}.*

(c) Anchoring energy measurement of liquid crystal molecules on a polymeric aligning surface

A film of liquid crystal molecules lying between two aligning surfaces can be properly modeled by continuum mechanics. The deformation of liquid crystal medium, the interaction of liquid crystal with an external field and alignment surface can be described with proper free energies

$$
\begin{aligned}
&F = f_b + f_f + f_s \quad where \\
&f_b = \frac{1}{2}\{k_{11}(\nabla \cdot \hat{n})^2 + k_{22}(\hat{n} \cdot \nabla \times \hat{n} + \frac{2\pi}{p_0})^2 + k_{33}[\hat{n} \times (\nabla \times \hat{n})]^2\} \\
&f_s = -\frac{1}{2} A (\hat{n} \cdot \hat{e})^2 \\
&f_f = -\frac{1}{2} \varepsilon_0 \, \Delta\varepsilon \, (\hat{n} \times E)^2
\end{aligned}
\quad . \qquad \text{(IIIc.1)}
$$

Here k_{11}, k_{22}, k_{33} are the splay, twist and bend elastic constants of the liquid crystal, respectively, and p_0 denotes the pitch of the material induced by a chiral dopant, and e represents the easy direction of the aligning surface. By minimizing the total free energy F with the Euler-Lagrange approach, the following equation can be obtained

$$
\begin{aligned}
&f(\theta)\frac{d^2\theta(z)}{dz^2} + \frac{1}{2}[\frac{df(\theta)}{d\theta}(\frac{d\theta}{dz})^2 - \frac{dh(\theta)}{d\theta}(\frac{d\phi}{dz})^2] + \varepsilon_0 \Delta\varepsilon \, E^2(z)\sin\theta(z)\cos\theta(z) = 0 \\
&\quad where \\
&f(\theta) = k_{11}\cos^2\theta + k_{33}\sin^2\theta
\end{aligned}
\qquad \text{(IIIc.2)}
$$

The solution $\theta(z)$ is subjected to the boundary conditions at z=0 and z=d

$$
\begin{aligned}
&f(\theta)\frac{d\theta}{dz}\Big|_{z=0} = -\frac{1}{2} A \sin[2(\theta - \theta_e)]\Big|_{z=0} \\
&f(\theta)\frac{d\theta}{dz}\Big|_{z=d} = \frac{1}{2} A \sin[2(\theta - \theta_e)]\Big|_{z=d}
\end{aligned}
\quad . \qquad \text{(IIIc.3)}
$$

The phase of a light beam after passing through a liquid crystal cell, which is excited with an external electric field, can be retarded with a magnitude of

$$
R = \frac{2\pi d}{\lambda}\left[\frac{n_\parallel n_\perp}{\sqrt{n_\parallel^2 \sin^2\theta + n_\perp^2 \sin^2\theta}} - n_\perp\right]. \qquad \text{(IIIc.4)}
$$

A set of calculated curves of R as a function of inverse voltage are presented in Fig. IIIb.1. It shows the anchoring strength A can be deduced from a saturated voltage, with that field strength all the liquid crystal molecules including that lie on the aligning surfaces are oriented perpendicularly with the electric field. Therefore with the saturated field strength, the optical retardance induced by liquid crystal film becomes zero. Experimentally the

saturated voltage can be estimated from the measured R-1/V curve by linearly expolating to the zero retardance point, and the anchoring strength can be calculated from

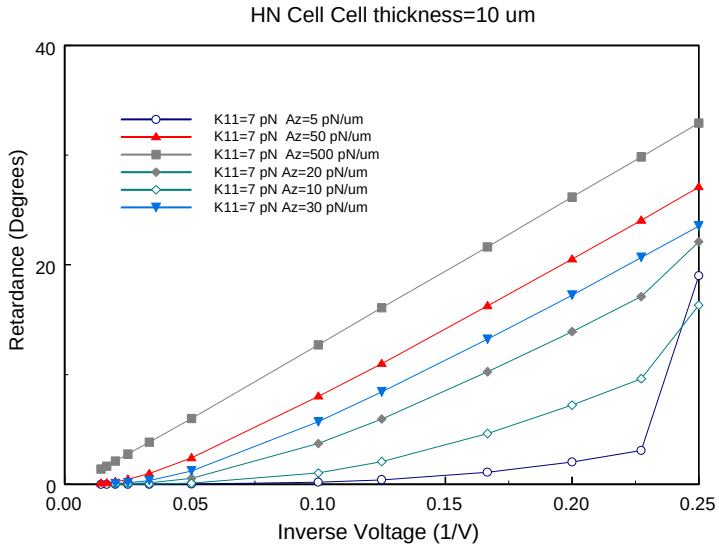

Fig. IIIc.1 *Calculated curves of optical retardance as a function of inverse voltage for anti-parallel aligned nematic liquid crystal cells with varying magnitudes of elastic constant* k_{11} *and anchoring strength A.*

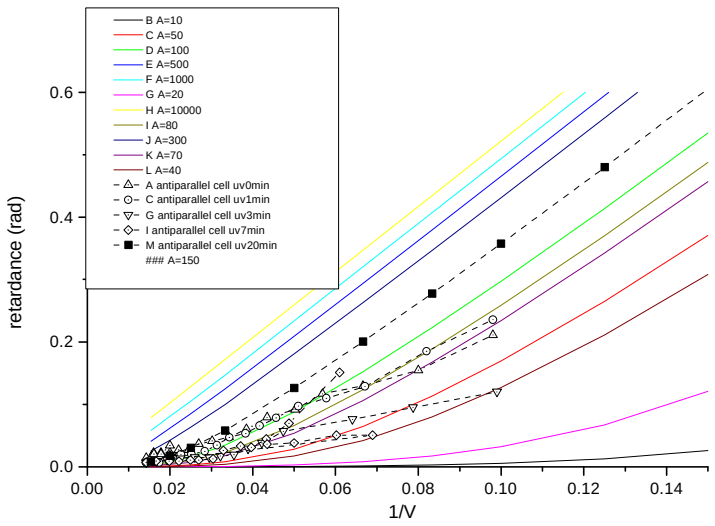

Fig. IIIc.2 *Measured (symbols) and calculated (lines) optical retardance of anti-parallel homogeneous nematic liquid crystal cells aligned by rubbed RN-1182 films with various anchoring energies.*

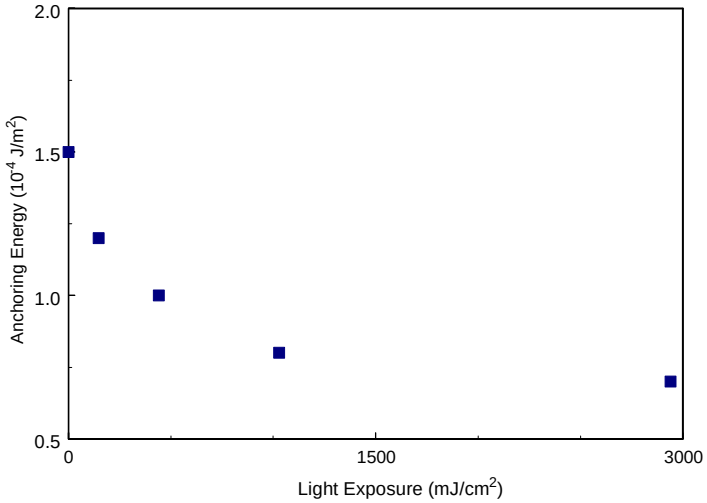

Fig. IIIc.3 *Measured anchoring energy of homogeneous nematic liquid crystal cells deduced from Fig. IIIc.2. The aligning surfaces were prepared by rubbed RN-1182 films and then subjected to various unpolarized UV light exposures.*

To determine the azimuthal anchoring strength imposed by rubbing action or linearly polarized ultraviolet light irradiation, 90^0-twist nematic liquid crystal cell were employed. Owing to an elastic torque from the twist LC bulk, the liquid crystal molecules on the surfaces do not orient to yield perfect $\phi_t = 90^0$ twist angle. Instead, there exists an angular deviation ϕ_0 with $\phi_t - 2\phi_0 - \frac{2\pi d}{p_0} = \frac{Ad}{k_{22}} \sin\phi_0 \cos\phi_0$. (IIIc.5)

Equation (IIIc.5) may give us the simplest way to evaluate the azimuthal anchoring strength. In other words, the anchoring energy can be calculated from the measurement of ϕ_0 as a zero-field technique.

We also investigate the molecular alignment of nematic liquid crystal molecules on UV light defined RN-1182 aligning surface with Raman spectroscopy. The aligning surfaces were exposed with linearly polarized ultraviolet light (LPUV) to induce in-plane anisotropy [7]. The stretching modes of the C=C and CN groups in a cyano biphenyl liquid crystal

molecule can be aligned by LPUV exposed polymer films. This is supported by the observed strong dependence of the Raman peaks on the rotational angle of the liquid crystal film along the surface normal as shown by Fig. IIIc.4.

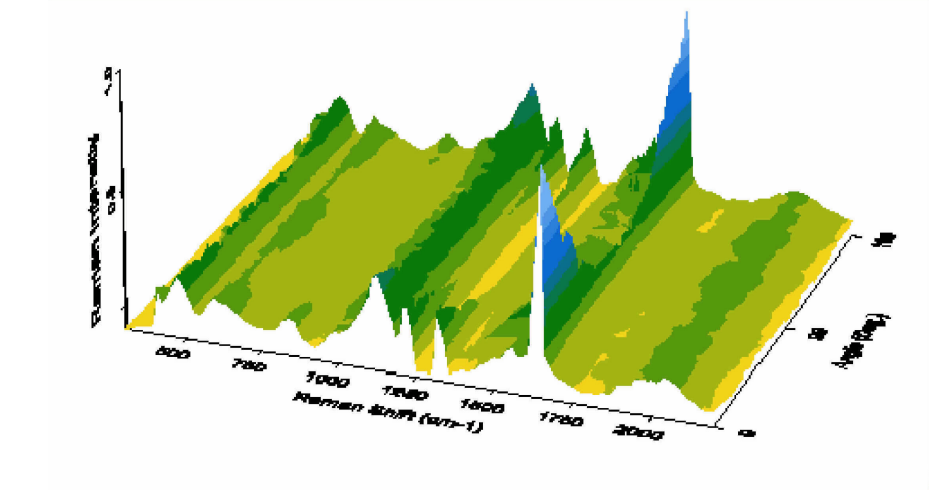

Fig. IIIc.4 *Raman spectra from a nematic cyano biphenyl liquid crystal film as a function of the rotation angle of the film relative to the surface normal. The zero degree denotes the anisotropic direction of the aligning layer.*

The molecular structure of cyano biphenyl liquid crystal molecule is shown in Fig. IIIc.5. We performed an *ab initio* density functional calculation to obtain the molecular vibrations and infrared absorption spectrum. The results are presented in Table IIIc.1

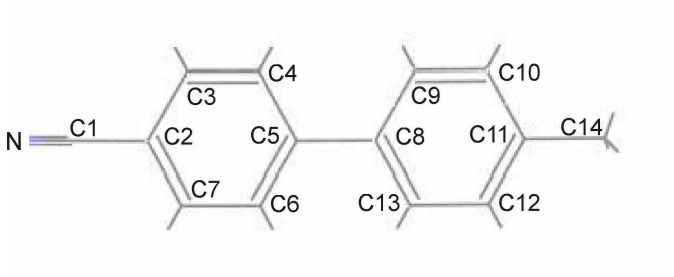

Fig. IIIc.5 *Schematic showing the molecular structure of cyano biphenyl (CB) liquid crystal*

Four peaks at 1200, 1302, 1616, and 2260 cm-1 can be attributed to from vibrations involved biphenyl and C-N stretches whose transition moments are mainly along the molecular long axis. If the long axes of liquid crystal molecules are aligned properly, their Raman scattering intensities should exhibit significantly azimuthal dependence.

Table IIIc.1 *Calculated molecular normal-mode frequencies of cyano biphenyl and the corresponding infrared absorption strengths*

Normal Modes	Vibration Frequency (cm^{-1})	IR Absorption	Symmetry
1. C_1-N stretch	2237	89.8	A_1
2. biphenyl C=C stretch	1605	46.3	A_1
3. (a) biphenyl C-C + C-H in-plane wag	1446	29.5	A_1
(b) C_5-C_8 stretch + C-H in-plane wag	1261	6.5	A_1
4. C(biphenyl)-H in-plane wag	1095	13.9	A_1
1. biphenyl in-plane angular distortion	985 510	4.2 5.9	A_1
6. C-H out-of-plane wag	507 544 664 713 742 818	9.9 6.3 42.8 11.8 45.7 23.2	B_1

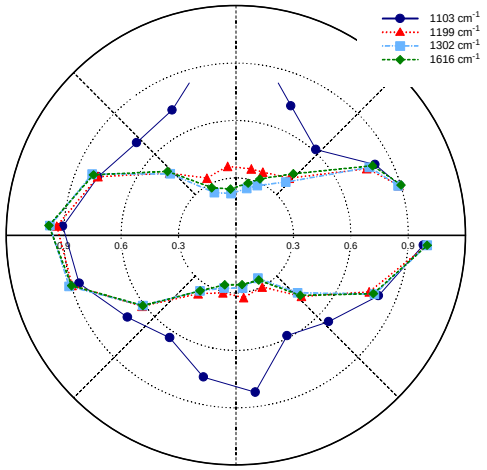

Fig. IIIc.6 Polar plot of *Raman peaks from a nematic cyano biphenyl liquid crystal film as a function of the rotation angle of the film relative to the surface normal.*

To probe the ordering, we select the C=C (biphenyl) stretch mode at 1616 cm-1 for further analysis. The order parameter of the liquid crystal molecules, which are sandwiched between two polymeric aligning surfaces, can be deduced by using Eq. (IIb.3). The results are presented in Fig. IIIc.7. Here the polymeric surfaces are rubbed uniaxially and then assembled anti-parallel. The rubbed surfaces were exposed to unpolarized UV light with various exposures. It is surprising to see that the unpolarized light exposure enhances the molecular alignment order instead of destroying it. Light exposure may remove some local defects from mechanical rubbing, thus increase liquid crystal ordering. Detailed information can be obtained by employing infrared-visible sum-frequency (IVSFG) vibration spectroscopy, which is well known for its outstanding surface sensitivity and molecular specificity. The study with IVSFG has been undertaking.

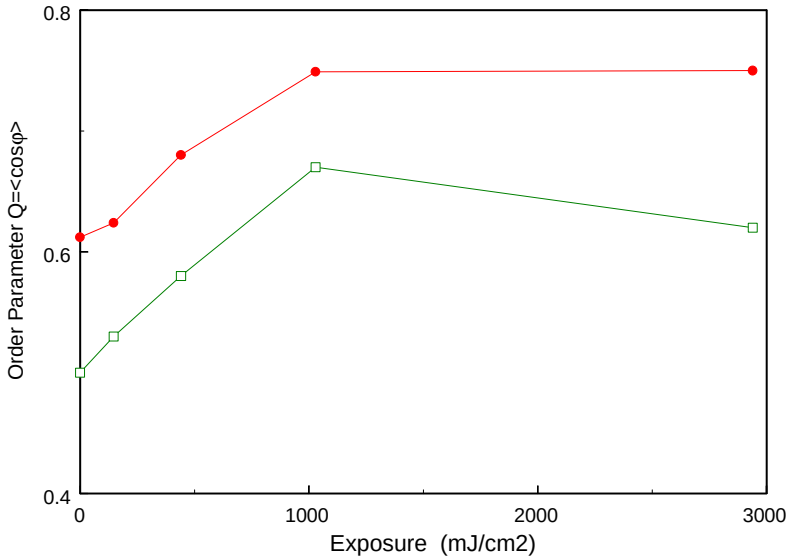

Fig. IIIc.7 Order parameter of the 1616 cm^{-1} *Raman peak from a homogeneous nematic liquid crystal film at 22 °C (red) and 33 °C (green). The Rubbed polymeric surfaces had been illuminated with unpolarized UV light to various exposures.*

(d) Raman imaging for thin complex films

Quantitative optical spectroscopic technique is highly useful for probing various optical properties of materials. Methods based on the generation of second harmonic (SH) light [1] and Raman scattering [2] are known to be capable of producing information about the polar orientation and composition of the sample being studied. In a typical measurement, a sample is illuminated with a focused laser beam and the generated SH or Raman signal is detected. The generated signal is then integrated over whole laser beam and pulse duration. The signal carries information about the material's properties averaged over the illuminated area. To probe the local structure and composition of a material, various imaging techniques should be employed for providing the spatial resolving ability[2,3].

In this section, we shall present a multifunctional optical microscopy with wide field illumination and multichannel detection. The analytical capability of our instrument was demonstrated with several application examples in which the polar structure and composition distribution of materials were resolved.

The Raman imaging spectro-microscope is detailed in Fig. IIId.1. Briefly, laser excitation is provided by a 523 nm doubled Nd:YLF laser and a wide field excitation is achieved at the sample. The scattered Raman photons are collected by an infinity-corrected microscope (Nikon, Eclipse 600) via a Raman edge filter (Omega Optical). For Raman imaging with high spatial fidelity, the Raman emission is filtered with a compact electronically controlled 8-cm^{-1} band pass liquid crystal tunable filter (LCTF)[4]. Raman images are collected using a 16-bit, TE-cooled (-20 ^{o}C), slow scan charge-coupled device (CCD) detector (Apogee, AP7) having 512 pixels $\times$ 512 pixels (25 μm). The CCD has quantum efficiency more than 80% from 500 nm to 800 nm.

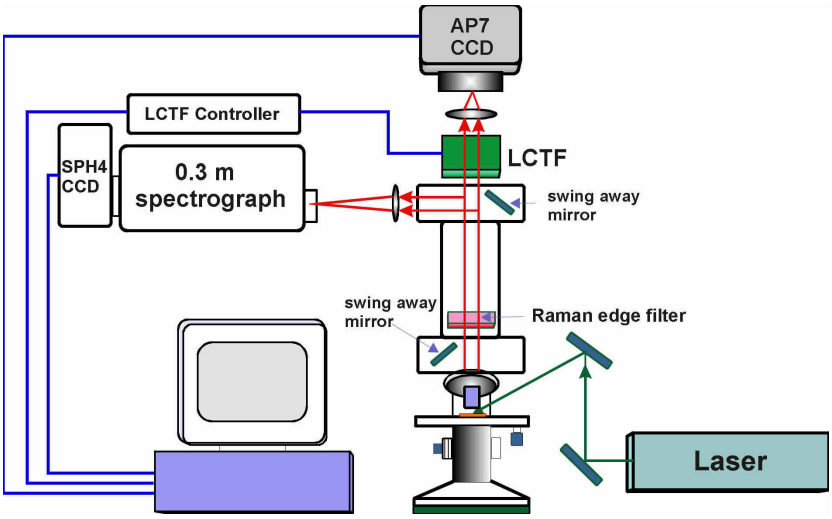

Fig. IIId.1 *Schematic of a Raman spectroscopy and microscope.*

A swing away mirror can be positioned before LCTF to redirect the Raman emission to a single-stage 0.3m spectrograph (Acton SP300). The Raman spectrum is collected with a CCD detector (Apogee, SPH4) located at the exit focal plane of the spectrograph.

For SH imaging, a compact mode-locked Nd:YAG laser with a repetition rate of 100 MHz and pulse duration of 18 ps is used [5]. The experimental setup is similar to that described in Fig. IIId.1 except transmission geometry is employed. A lens with a focal length of 50 cm focuses the fundamental beam at 1.064 «m to achieve a peak power of 250 MW/cm^2. The second harmonic signal at 532 nm was separated from the fundamental with a series of filters in order to obtain high signal-to-noise ratio.

For probing the material composition, vibrational spectroscopy is better suited than absorption/luminescence spectroscopy owing to its finger printing capability. By combining Raman spectroscopy with optical microscopy, a distribution of material composition can be revealed. This is illustrated in Fig. IIId.2, where Raman spectrum and Raman image from a silicon integrated circuit chip are presented. The sample had subjected to various oxidation and metallization processes. The Raman spectrum showed in Fig. IIId.2 (a) exhibits three peaks located at 520, 610 and 810 cm^{-1}. The 520-cm^{-1}-peak is originated from the lattice

vibration of single crystal silicon (SCS) substrate. The other two peaks are mainly from silicon and oxygen bonding as their intensities are much enhanced compared with the spectrum taken on a clean SCS (bottom) with a native oxide.

By tuning the LCTF to the corresponding wavelengths of the Raman peaks, the two-dimensional intensity distributions of the Raman signals can be obtained. In Fig. IIId.2(b), the color composite (red=520 cm^{-1}, blue=620 cm^{-1}, green=820 cm^{-1}) Raman chemical image of the sample is presented to reveal the composition distribution of silicon and oxide on the chip.

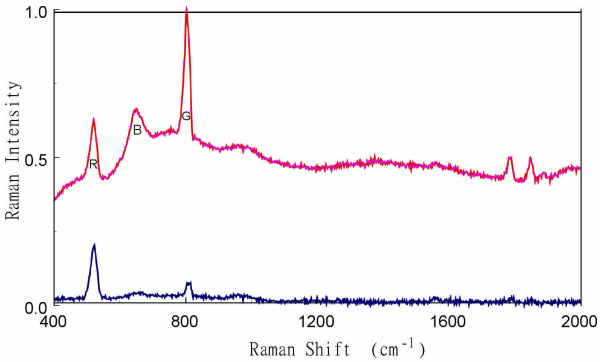

(a) Raman Spectrum

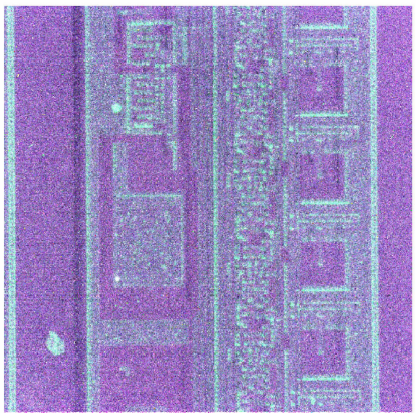

.

Fig. IIId.2 (a) *Raman spectrum from a silicon integrated circuit chip (top) and a single crystal silicon substrate (bottom). (b) Color composite Raman chemical image of the 520 cm^{-1} (red), 610 cm^{-1} (blue) and 810 cm^{-1} (green) peaks from the silicon integrated circuit chip.*

In summary, a multifunctional optical microscope has been developed for spatially resolving the second harmonic and Raman scattering photons. The instrument has been successfully applied to reveal the polar structure and composition distribution of some

optical materials. Detailed analysis of these imaging data demonstrates the technique to be useful for many other functional materials with high application potential.

REFERENCES

[1] Y. R. Shen, Nature (London) **337**, 519 (1989).

[2] H. R. Morris, J. F. Turner, H. Branka, M. Rose, A. Ryntz, and P. J. Treado, *Langmuir* **15**, 2961-2972 (2000).

[3]M. H. Flörsheimer, M. Salmen, C. Bösch, M. Brillert, M. Wierschem, and H. Fuchs, *Adv. Mater.* **9**, 1061-1065 (1997); J. Vydra, and M. Eich, *Appl. Phys. Lett.* **72**, 275-277 (1998).

[4]K. A. Christensen, N. L. Bradley, M. D. Morris, and R. V. Morrison, *Appl. Spectrosco.* **49**, 1120-1125 (1995).

[5]P. K. Yang and J. Y. Huang, *Opt. Commun.* **173**, 315-321 (2000).

[6]Pao-Keng Yang, Jung Y. Huang, and Jwo-Huei Jou, *Proc. of NSC* **A 24,** 310-315 (2000).

K. Sakamoto, K. Usami, T. Araya, and S. Ushioda, *Jpn. J. Appl. Phys.* **38**, L1435-L1438 (1999).

(e) Time-resolved polarized Fourier-transform infrared absorption spectroscopy for liquid crystal alignment and field-induced reorientation

Vibrational spectroscopy, such as Raman and infrared absorption spectroscopies, are better suited for probing molecular conformation owing to the finger printing capability. In liquid crystal research, an important question is that how liquid crystal molecules are aligned and reoriented during field-induced switching. It is still unclear for the detailed reorientation dynamics of chain and core parts of liquid crystal. Time-resolved Fourier transform infrared absorption spectroscopy could yield more useful information.

Recently, Masutani *et al.* [Appl. Spectro. 46, 560 (1992)] developed a novel asynchronous time-resolved FTIR spectrophotometer based on a conventional continuous-scan interferometer. Their new method does not require synchronization between the signal for time resolving and that for the sampling of the AD converter. In addition, there is no shortest limit in time for transient phenomena to be measured, therefore time-resolved

measurements in the nanosecond or even shorter could be possible if proper gating technique with infrared laser pulses are available.

In these regards, we modify a commercial FTIR module for making it a time-resolved FTIR spectrophotometer in order to answer how liquid crystal molecules are aligned and reoriented during field-induced switching processes. The schematic of our time-resolved FTIR set up is described in Fig. IIIe.1. The electronic modules in blue color are involved in the original FTIR modules. The resulting signals at every labeled point are depicted in Fig. IIIe.2.

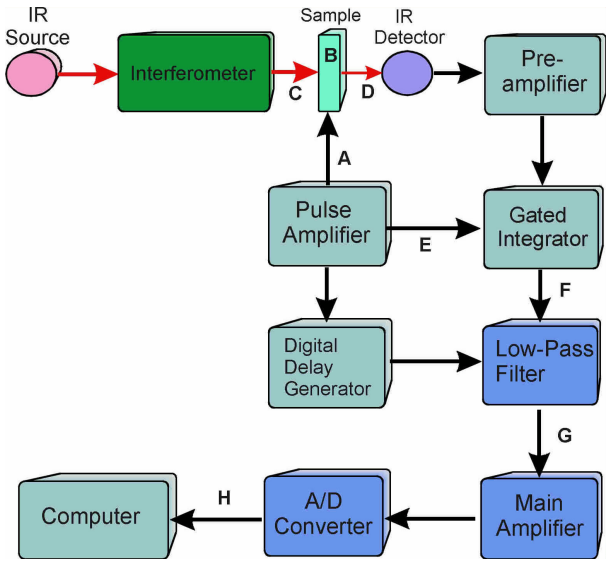

Fig. IIIe.1 *Schematic showing a time-resolved Fourier transform infrared absorption spectroscopy with asynchronous continuous scan approach.*

Consider a material, which is excited by a periodic excitation $\Pi_{\tau}(t)$ (see Fig. IIIe.2**,** **A**) and the recovery time of the material is shorter than τ. The infrared transmittance through the excited sample at time t is given then by

$$T(\neg, t) = T_0(\neg) + \Delta T(\neg, t) \otimes \Pi_{\tau}(t) \qquad \text{(IIIe.1)}$$

We can also properly express the resulting interferogram as

$$
\begin{aligned}
F(x=2vt_m,t) &= \int_{-\infty}^{+\infty} T_0(\neg,t)S(\neg)\cos[2\pi x\neg]d\neg + \int_{-\infty}^{+\infty}\Delta T(\neg,t)\otimes\Pi_\tau(t)S(\neg)\cos[2\pi x\neg]d\neg \\
&= \int_{-\infty}^{+\infty} T_0(\neg,t)S(\neg)\cos[2\pi x\neg]d\neg + \int_{-\infty}^{+\infty}[\int\Delta T(\neg,t-t')\sum_{n=-\infty}^{+\infty}\delta(t'-n\tau)dt']S(\neg)\cos[2\pi x\neg]d\neg \\
&= \int_{-\infty}^{+\infty} T_0(\neg,t)S(\neg)\cos[2\pi x\neg]d\neg + \int_{-\infty}^{+\infty}\sum_{n=-\infty}^{+\infty}\Delta T(\neg,t-n\tau)S(\neg)\cos[2\pi x\neg]d\neg
\end{aligned}
\qquad \text{(IIIe.2)}
$$

By employing a gating technique to sample the interferogram at a fixed delay time Δt_D=gate-excitation, the time resolved interferogram (see Fig. IIIe.2**, F**) becomes

$$
\begin{aligned}
F'(x,t) &= G_\tau(t-\Delta t_D)[\int_{-\infty}^{+\infty} T_0(\neg)S(\neg)\cos[2\pi\nu x)d\neg + \int_{-\infty}^{+\infty} S(\neg)\cos[2\pi\nu x)\sum_{n=-\infty}^{+\infty}\Delta T(\neg,t-n\tau)d\neg \\
&= G_\tau(t-\Delta t_D)\int_{-\infty}^{+\infty} T(\neg,\Delta t_D)S(\neg)\cos[2\pi\nu x)d\neg
\end{aligned}
$$

(IIIe.3)

where $T(\nu, \Delta t_D)$ denotes the time-resolved transmittance at the delay time Δt_D. A smooth time-resolved interferogram can be obtained by passing the gated signal through a low pass filter (see Fig. IIIe.2**, G**)

$$
F(x,\Delta t_D) = \frac{1}{2}\int_{-\infty}^{+\infty} T(\neg,\Delta t_D)S(\neg)\cos[2\pi\nu x)d\neg \qquad \text{(IIIe.4)}
$$

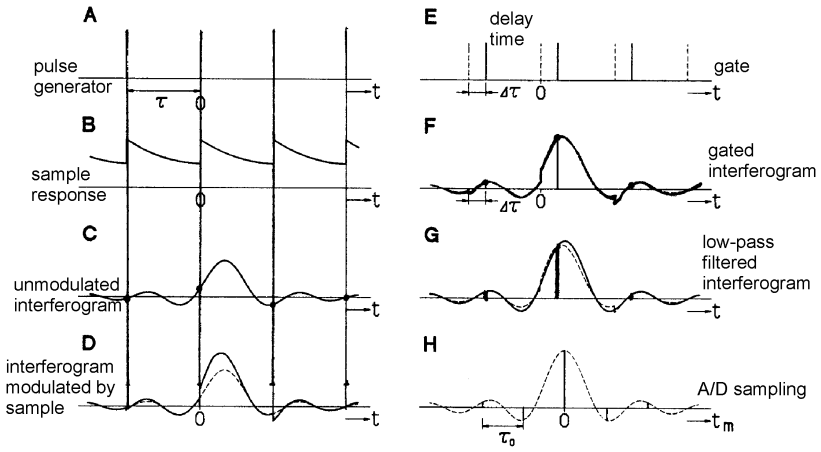

Fig. IIIe.2 *Schematic showing signals at each step of the time-resolved Fourier transform infrared absorption spectroscopy.*

We have checked the signals to be properly produced at each step. The data acquisition in the time-resolved FTIR does not distort the acquired interferograms. This is confirmed in Fig. IIIe.3, where two the infrared absorption spectra of a polyimide film for homeotropic liquid crystal alignment measured with a continuous scan (blue color) and the time-gating setup (red color) are compared. The gating circuit reproduces all the fine features of the spectrum obtained by a continuous-scan FTIR module.

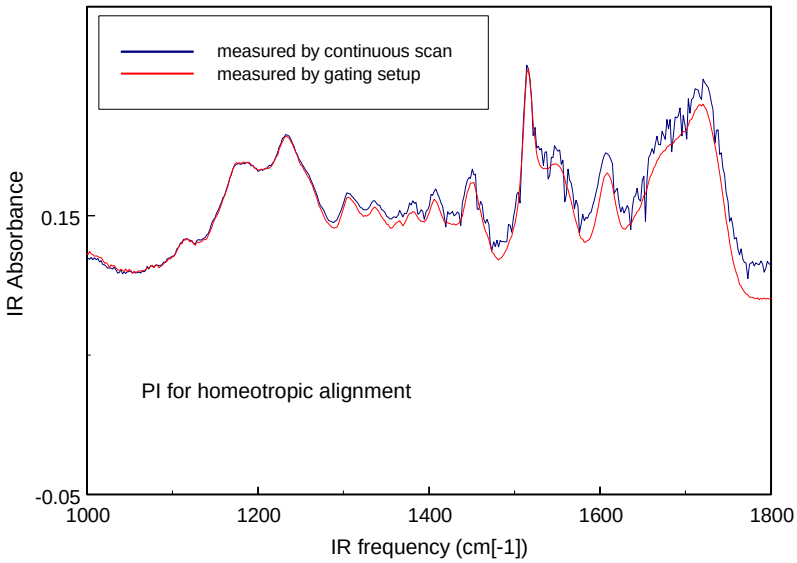

Fig. IIIe.3 *Fourier-transform infrared absorption spectra of a polyimide film measured with a continuous-scan FTIR module (blue) and with gating circuit inserted (red).*

IV. **Conclusions and future prospect**

In this report, we present the studies of complex thin films, such as liquid crystals and polymeric aligning layers, with optical retardance measurement, infrared absorption spectroscopy, Raman scattering, and Raman imaging microscopy. The molecular ordering of liquid crystals and polymeric thin films induced by mechanical rubbing and ultraviolet light exposure are chosen in view of their technical potential. An important question about their various applications is how liquid crystal molecules are aligned and reoriented during

field-induced switching. It is still unclear for the detailed reorientation process of chain and core parts of liquid crystal. To understand the underlying dynamics at the molecular level, we are currently employing Fourier transform infrared absorption spectroscopy to generate time resolved FTIR spectra of liquid crystal molecules during the field-induced switching process. By combining these techniques we wish in the near future to answer how molecular chirality and chiral dopants affect the switching dynamics of ferro- and antiferroelectric liquid crystals.